Pis'ma v ZhETF, vol. 80, iss. 3, pp. 174 – 178

Topological noise scalings in superfluid and classical turbulence

D. Kivotides[1)]

Low Temperature Laboratory, Helsinki University of Technology, FIN-02015 HUT, Finland

Submitted 2 July 2004

We calculate the topological noise characterizing the direction of line vortices in superfluid and classical turbulence by finding the intersection of line vortices with square surfaces of edge length l_s positioned normal to three orthogonal axes. In the case of homogeneous superfluid turbulence in thermal counterflow, we find that the noise scales like l_s along the two directions normal to the counterflow and like $l_s^{3/2}$ along the direction parallel to it. In homogeneous isotropic superfluid turbulence at $T \to 0\,\mathrm{K}$, the noise scales like $l_s^{7/4}$. In homogeneous isotropic classical turbulence the scaling is l_s^2. We offer possible interpretations of the computed scalings, as well as, justification for their differences.

PACS: 47.27.Gs, 47.32.Cc, 67.40.Vs

Turbulence in thermally excited superfluids involves the interaction of topological defects (line vortices) of collective superfluid motion with thermal excitations of the superfluid ground state (normal fluid) via mutual friction forces. In the related field of classical turbulence, a quantized model of Navier–Stokes turbulence was developed in which all flow vorticity is in the form of classical vortex filaments (schoinoidal turbulence). The model was found to reproduce central aspects of classical turbulence phenomenology like Kolmogorov scalings for the second and third order structure functions [1], Navier–Stokes turbulence kinematics [2] and geometrical aspects of turbulent vorticity [3]. Definitely, in all cases the geometry of the vortices is of paramount importance. However, much less detailed information might be of importance in cases where gross properties of the system are of interest [4 – 6]. For example, the (topological) noise characterizing the direction of vortices intersecting a particular surface dividing in two the fluid volume, provides information about the net vorticity flux through the surface. Moreover, noise scalings are important in the context of quantum field theory (condensed matter and high energy physics), where changes in asymptotic scaling behavior mark phase transitions [7]. In this Letter, we investigate whether topological noise scalings exist in the context of flow turbulence and how they might be affected by the equations of motion. We study three different flow situations: (a) homogeneous superfluid turbulence in thermal counterflow [8, 9], (b) homogeneous isotropic superfluid turbulence at $T \to 0\,\mathrm{K}$ [10] and (c) homogeneous isotropic classical turbulence.

(a) The mathematical system describing thermal counterflow concerns exclusively the quantized vortex dynamics. This is because the counterflow velocity $\mathbf{V}_n - \mathbf{V}_s$ itself (with $\mathbf{V}_n$ the normal fluid velocity and $\mathbf{V}_s$ the irrotational part of superfluid velocity) is kinematically imposed. Therefore, although the counterflow affects the line vortex motion, it is unaffected by the latter. If $\mathbf{S}(\xi, t)$ is the three dimensional representation of the vortex tangle (where ξ is the arclength parametrization along the loops and t is time), then its motion obeys the equation [11]:

$$\frac{d\mathbf{S}}{dt} = \mathbf{V}_l = \mathbf{V}_s + \mathbf{V}_{bs} + \alpha_x \mathbf{S}' \times (\mathbf{V}_n - \mathbf{V}_s - \mathbf{V}_{bs}) - \\ - \alpha_{xx} \mathbf{S}' \times [\mathbf{S}' \times (\mathbf{V}_n - \mathbf{V}_s - \mathbf{V}_{bs})] \qquad (1)$$

where the rotational part of superfluid velocity $\mathbf{V}_{bs}$ is given by the Biot-Savart integral:

$$\mathbf{V}_{bs}(\mathbf{x}) = -\frac{\kappa}{4\pi} \int d\xi \frac{\mathbf{S}' \times (\mathbf{S} - \mathbf{x})}{|\mathbf{S} - \mathbf{x}|^3}. \qquad (2)$$

There $\mathbf{x}$ is the space coordinate, κ is the quantum of circulation, $\mathbf{S}' = d\mathbf{S}/d\xi$ is the unit tangent vector and α_x, α_{xx} are the mutual friction coefficients.

The working fluid is ^{4}He and the temperature $T = 1.3\,\mathrm{K}$. Under these conditions $\kappa = 9.97 \cdot 10^{-4}\,\mathrm{cm}^2/\mathrm{s}$, the density of the normal fluid is $\rho_n = 6.5 \cdot 10^{-3}\,\mathrm{g/cm}^{-3}$, the density of the superfluid is $\rho_s = 138.6 \cdot 10^{-3}\,\mathrm{g/cm}^{-3}$, the normal fluid viscosity is $\nu = 23.30 \cdot 10^{-4}\,\mathrm{cm}^2/\mathrm{s}$, $\alpha_x = 3.4145 \cdot 10^{-2}$ and $\alpha_{xx} = 1.3703 \cdot 10^{-2}$. The computation is done in a box of size $l_b = 0.1\,\mathrm{cm}$ with periodic boundary conditions to enforce homogeneity. The velocities $\mathbf{V}_n$ and $\mathbf{V}_s$ are prescribed to be parallel to the y axis. We prescribe the Reynolds number of the normal fluid $\mathrm{Re} = |\mathbf{V}_n| l_b/\nu$ at $t = 0$ to be $\mathrm{Re} = 50$. This specifies $|\mathbf{V}_n| = 0.6408\,\mathrm{cm/s}$ and using the continuity equation $\rho_s \mathbf{V}_s + \rho_n \mathbf{V}_n = 0$ we find $\mathbf{V}_s = -(\rho_n/\rho_s)\mathbf{V}_n$ with $|\mathbf{V}_s| = 0.030146\,\mathrm{cm/s}$. Then by specifying the initial geometry of the tangle (which at $t = 0$ consists of

[1)] e-mail: demos@galcit.caltech.edu

10 randomly positioned rings of length $L_0 = 2.1608\,\mathrm{cm}$), one can calculate the evolution of the tangle using numerical methods. We choose the discretization length $\Delta\xi$ along the line vortices to be $\Delta\xi = 2.0833 \cdot 10^{-3}\,\mathrm{cm}$ and the numerical time step Δt to be small enough so that no possible (resolved by $\Delta\xi$) Kelvin wave in the system propagates more than $\Delta\xi$ during Δt. This requirement leads to typical time steps $\Delta t \approx 0.001\,\mathrm{s}$. Finally, when two vortices approach closer than $\Delta\xi$ they reconnect. This methodology is supported by the results of [12, 13].

Knowledge at each time step of the tangle's configuration allows the calculation of topological number noise. The following algorithm was developed for this purpose. First, the average intervortex distance $l_\zeta = (L/l_b^3)^{-1/2}$ is defined. Subsequently (for sufficiently dense tangles), a range of length sizes is specified $[ml_\zeta, l_b]$ with m being a small natural number ($m = 4$ in the present calculation). A sequence of lengths l_s ($ml_\zeta < l_s < l_b$) is generated by dividing $[ml_\zeta, l_b]$ into n subintervals ($n = 100$ in this computation). Each of the lengths l_s in this sequence is taken to be the edge of a square surface positioned normal to each axis in due order of succession. For each choice of edge length and axis, we consider k surfaces ($k = 1000$ in this calculation). The position of each square surface center is defined using random numbers for the coordinates. For every surface, we determine the intersection points with the vortex tangle. In doing this, we attribute to every intersection point a topological number $+1$ or -1 depending on whether the vorticity vector is pointing towards one or the other of the two halfs of the fluid volume that the surface delimits. In this work, the number $+1$ is used when vorticity points towards the positive part of an axis. We call these numbers topological because they characterize the direction of vorticity vector along the line vortex and this direction, as well as, the vortex itself persist in time due to the topological nature of the defects. We define N^+ to be the sum of points associated with topological number $+1$ and in a similar way we define N^-. In the end, the above mentioned exercise attributes to each surface the quantity $N^+ - N^-$ which represents the net number of vorticity vectors that thread the surface possesing one of the two possible orientations. By squaring this quantity and averaging over the number k of surfaces of edge l_s normal to the particular axis, we obtain the topological (number) noise $\theta_i(l_s) = \langle (N^+ - N^-)^2 \rangle$ with $i = 1, 3$ representing the three directions.

In accordance with the calculations of [14] the counterflow causes a rapid increase in the tangle length L. At $t = 9.7\,\mathrm{s}$, $L = 182.9\,\mathrm{cm}$ and due to the dramatic increase in the number of vortex particles required by the numerics, the calculation becomes very complex. In response to this, we regulate the magnitude of the counterflow in order to achieve a steady state for L. We find (Fig.1, top) that when the Reynolds number is close

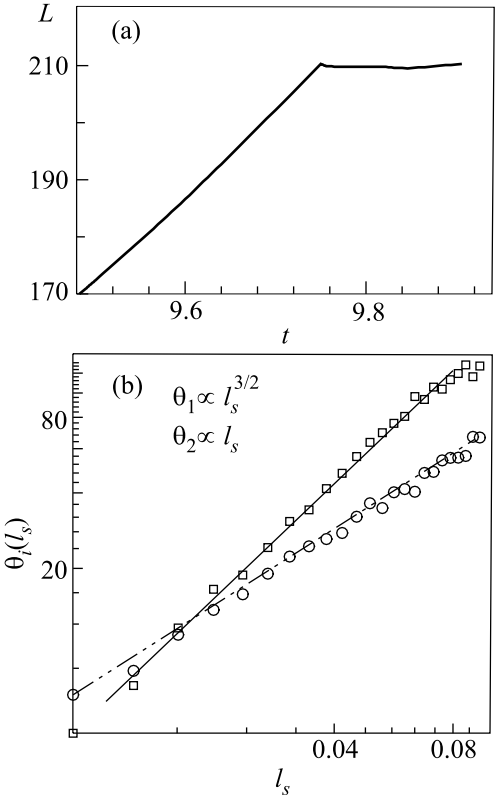

Fig.1. Results for counterflow turbulence: Time evolution of tangle length L (top) and topological noises θ_i as functions of the surface edge length l_s at stoppage time (bottom). Time t is measured in s and L, l_s in cm

to $\mathrm{Re} = 27.5$ the tangle length becomes to a very good approximation stationary. Definitely, one would like to continue the calculation for longer times while keeping the vortex length approximately constant. However, for the number of particles in the present calculation (typically close to $80 \cdot 10^3$), the Biot-Savart many body problem is computationally too complex for that. This situation might change in the future with the combination of powerful numerical (tree algorithms) and computational (parallel algorithms) methodologies. It is observed (Fig.1, bottom) that over a decade of l_s, θ_1 and θ_2 display the scaling behaviour l_s and $l_s^{3/2}$ respectively. We note that θ_2 refers to surfaces normal to the counterflow and that the θ_1 and θ_3 scaling behaviours were identical. The scalings remained unaltered throughout the time interval of approximately constant L. The noise in the counterflow direction seems to be proportional to

the measure of a fractal object thicker than a line but still not as extented as a surface.

One can say that the counterflow introduces an anisotropy in the equations of motion. Indeed, in contrast to vortices along the x and z directions, those parallel to $\mathbf{V}_n - \mathbf{V}_s$ do not interact with the counterflow. Therefore, as far as, the tangle configuration is concerned, a kind of order is introduced along the normal to the counterflow axes due to the $\mathbf{S}' \times (\mathbf{V}_n - \mathbf{V}_s)$ terms in the equations of motion. As a result, different scalings are observed in different directions although the particular values of the observed scalings are not a priori anticipated. Certainly since $\mathbf{V}_n - \mathbf{V}_s$ drives the turbulence in the system, one should not exclude the possibility that the calculated exponents depend on the counterflow velocity magnitude. How should one interpret the $l_s^{3/2}$ scaling? It is possible that since the counterflow velocity does not interact with vortices parallel to $\mathbf{V}_n - \mathbf{V}_s$ this scaling is indicative of the situation where $\mathbf{V}_n - \mathbf{V}_s = 0$ but there is still mutual friction. In this case, the only relevant velocity for the determination of the speed of the line vortex is the Biot-Savart one. However, one can object arguing that the $l_s^{3/2}$ scaling incorporates indirectly the effect of the counterflow due to the interdependence of the vortex dynamics along the three dimensions which leads to influence from the more orderly vortex states along the other two directions. Certainly, future computations could clarify these important issues.

(b) The mathematical system that describes superfluid turbulence for $T \to 0$ in the absence of any irrotational flow component is a subset of equation (1):

$$\frac{d\mathbf{S}}{dt} = \mathbf{V}_{bs} \tag{3}$$

with $\mathbf{V}_{bs}$ defined as in equation (2). The size of the box is the same as before $l_b = 0.1\,\text{cm}$. The discretization length $\Delta\xi$ along the line vortices is $\Delta\xi = 1.1904 \cdot 10^{-3}\,\text{cm}$ and the numerical time step Δt is $\Delta t \approx 0.001\,\text{s}$. There are initially 700 randomly positioned vortex rings of total length $L = 86.39\,\text{cm}$. The temporal evolution of L is seen in Fig.2 (top), indicating a steady state. The latter is not surprising since the superfluid vortex system is conservative and its energy is constant in time hinting at small variations of the tangle length. Until stoppage time, around 500 reconnections have occured in the system and 50 time steps were taken. Since (by construction) the flow is homogeneous and isotropic, the topological noises θ_i $i = 1, 3$ were found to be similar in all directions. Therefore in Fig.2 (bottom), we plot the arithmetic mean θ_a of the noises θ_i. It is evident that θ_a scales like $l_s^{7/4}$. We have checked that during the last

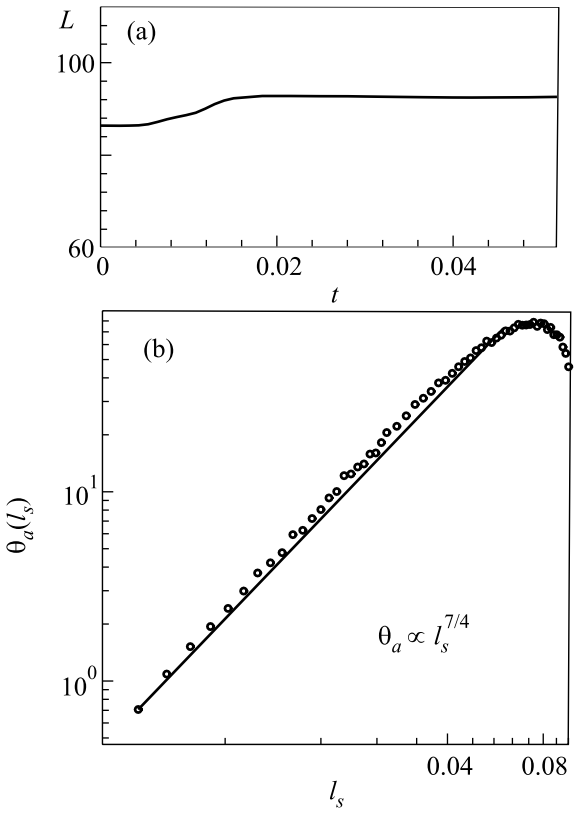

Fig.2. Results for homogeneous isotropic superfluid turbulence at $T \to 0$: Time evolution of tangle length L (top) and average of topological noises θ_a as function of the surface edge length l_s at stoppage time (bottom). Time t is measured in s and L, l_s in cm

ten time steps of the computation the scaling remained invariant. The contrast with the exponents calculated for counterflow turbulence is indicative of the different physics characterizing the two situations.

(c) Finally, the mathematical system that describes (the quantized model) of classical turbulence is also based on the Biot-Savart equation: If $\mathbf{r}_i$ is the three dimensional representation of the centre-line curve of filament i then the vortex motion is described by:

$$\frac{d\mathbf{r}_i}{dt} = \mathbf{V}(\mathbf{r}_i(t), t), \tag{4}$$

where $\mathbf{V}(\mathbf{r}_i(t), t)$ is the Biot-Savart velocity:

$$\mathbf{V}(\mathbf{x}, t) = -\frac{1}{4\pi} \int \frac{(\mathbf{x} - \mathbf{x}') \times \boldsymbol{\omega}(\mathbf{x}') d\mathbf{x}'}{|\mathbf{x} - \mathbf{x}'|^3} \tag{5}$$

with $\boldsymbol{\omega}(\mathbf{x}')$ being the vorticity vector and $\mathbf{x}'$ denoting points along the core centerlines. In case of superfluid topological defects, $\boldsymbol{\omega}(\mathbf{x}')$ is a delta-function along the curve of the vortex C_i since the superfluid vortices have

(at hydrodynamic scales) infinitesimal core sizes. However, in the classical Navier–Stokes case the vortices have dynamic, finite cores and the vorticity is distributed. Because of this we employ a more complex vorticity representation [16]:

$$\boldsymbol{\omega}(\mathbf{x}',t) = \sum_i \Gamma \int_{C_i} \frac{1}{\sigma_i(\xi,t)^3} \zeta\left(\frac{|\mathbf{x}' - \mathbf{r}_i(\xi,t)|}{\sigma_i(\xi,t)}\right) \times \\ \times \left(\frac{\partial \mathbf{r}_i}{\partial \xi} + \frac{\mathbf{x}' - \mathbf{r}_i(\xi,t)}{\sigma_i(\xi,t)} \frac{\partial \sigma_i}{\partial \xi}\right) d\xi, \qquad (6)$$

where $\sigma_i(\xi)$ is the local core radius of filament i and the smoothing kernel ζ describes the way vorticity spreads around the core centerline. There is a variety of smoothing kernels suitable for the computation. The high order algebraic kernel of [17] is the one used here. A detailed discussion of the numerical analysis and the formulas used can be found in [18]. Γ is the circulation strength attributed to all filaments and is the model's analog of the quantum of circulation. The formula shows that the vorticity field has two constituents. The first term of the sum inside the integral sign models the vorticity component along the direction of the filament tangent $\partial \mathbf{r}_i / \partial \xi$. This is the only component present in quantum vortices (without the smoothing effect of ζ). The second term models the vorticity component along the direction $\mathbf{x} - \mathbf{r}_i(\xi)$ and is induced by the change of $\sigma_i(\xi)$ along the filaments. The filament cores tend to grow due to diffusive effects. This phenomenon is calculated using the core-spreading method [19]. When two filaments approach within a certain distance from each other they reconnect. Detailed description of the reconnection methodology can be found in [20].

In order to calculate the topological noises we use the stoppage time tangle configuration of [3]. In this earlier calculation, the initial conditions consist of 192 rings in a periodic box. The Reynolds number has the value $\mathrm{Re} = \frac{\Gamma}{\nu} = 5 \cdot 10^3$. The results are made dimensionless in the following manner: $t = \frac{\Gamma t'}{R^2}$, $\mathbf{x} = \frac{\mathbf{x}'}{R}$, $\boldsymbol{\omega} = \frac{R^2 \boldsymbol{\omega}'}{\Gamma}$ where t', $\mathbf{x}'$, $\boldsymbol{\omega}'$ are dimensional and R is a reference initial vortex-ring radius. We have chosen $\Gamma = 1$ and $R = 1$; the box size is $l_b = 2.041$. The discretization length $\Delta\xi$ along the line vortices is $\Delta\xi = 4 \cdot 10^{-2}$ and the numerical time step Δt is $\Delta t \approx 0.0024$. In order to have a stable calculation, the latter is chosen to be the inverse of the maximum average vorticity over the vortex cores. The total evolution time is comparable to the life time of the large eddies. The temporal evolution of tangle length L after the artificial initial transient is shown in Fig.3 (top). As demonstrated in [1] this flow exhibits a Kolmogorov scaling exponent for the energy spectrum. Since the flow is isotropic, we have verified

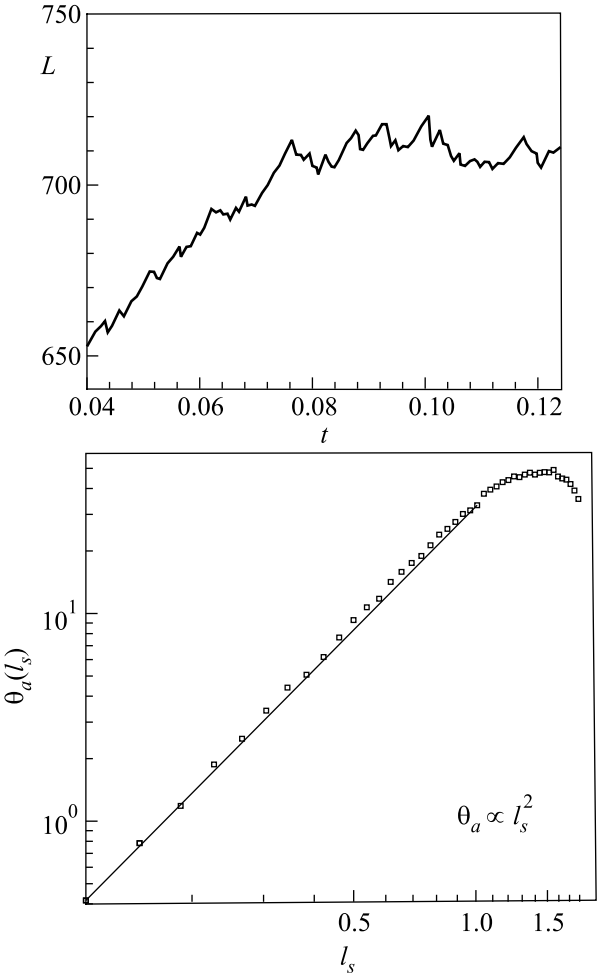

Fig.3. Results for homogeneous isotropic classical turbulence: Time evolution of tangle length L as calculated in [3] (top) and average of topological noises θ_a as function of the surface edge length l_s at stoppage time (bottom). All quantities are nondimensional

that all three dimensions give identical scalings. In Fig.3 (bottom) we plot the arithmetic mean θ_a of the noises θ_i. It is evident that θ_a scales like l_s^2. Why the difference in scaling exponents between classical and quantum case? After all is it not the case that both are described by the Biot-Savart integral? The answer to these questions could be found in [3, 15]. In these papers, the curvature spectra for superfluid and classical vortices were reported. In the former case it was found that the spectra were flat (white noise like). However, in the latter case a non-trivial scaling was discovered exactly in the wavenumber regime corresponding to the inertial range of turbulence with Kolmogorov scaling. The authors of [3] attributed this difference to the ability of classical vortices (in opposition to superfluid line vortices) to stretch. Therefore, since the geometries in

these two cases are different, there is no reason to expect the topological noise scalings (which are determined by the geometry) to be identical.

The scalings revealed in the present work are characterized by the simplicity of the computed quantities. It is desirable that a deeper (and more technical) study of possible connections between the physics of vortex systems and the topology/geometry of their configurations is pursued in the future (e.g. [21, 22]). Such studies would illuminate the mechanisms underlying the appearence of the observed scalings. Finally, one notes that due to computational complexity it is difficult to make the same calculation with a wide range of counterflow velocity magnitudes. Therefore, it is not possible at present to be assertive about the universality of the reported (counterflow) scaling exponents.

This research was supported by the Commission of the European Union under Contract # HPRI-CT-1999-00050. I thank Grigory Volovik for pointing out to me reference [5], Vladimir Eltsov and Matti Krusius for discussions, as well as, Caltech for computer resources.

1. D. Kivotides and A. Leonard, Phys. Rev. Lett. **90**, 234503 (2003).
2. D. Kivotides and A. Leonard, Europhys. Lett. **65**, 344 (2004).
3. D. Kivotides and A. Leonard, Europhys. Lett. **66**, 69 (2004).
4. A. Maniv, E. Polturak, and G. Koren, Phys. Rev. Lett. **91**, 197001 (2003).
5. G. E. Volovik, JETP Lett. **78**, 533 (2003).
6. G. E. Volovik, *The universe in a helium droplet*, Oxford University Press, 2003, p. 353.
7. A. M. Polyakov, *Gauge fields and strings*, Harwood Academic, Chur, 1987.
8. S. C. Courts and J. T. Tough, Phys. Rev. **B38**, 74 (1988).
9. A. P. Finne, T. Araki, R. Blaauwgeers et al., Nature **424**, 1022 (2003).
10. W. F. Vinen and J. J. Niemela, J. Low Temp. Phys. **128**, 167 (2002).
11. O. C. Idowu, D. Kivotides, C. F. Barenghi, and D. C. Samuels, J. Low Temp. Phys. **120**, 269 (2000).
12. J. Koplik and H. Levine, Phys. Rev. Lett. **71**, 1375 (1992).
13. A. T. A. M. de Waele and R. G. K. M. Aarts, Phys. Rev. Lett. **72**, 482 (1994).
14. K. W. Schwarz, Phys. Rev. **B38**, 2398 (1988).
15. D. Kivotides, J. C. Vassilicos, D. C. Samuels, and C. F. Barenghi, Phys. Rev. Lett. **86**, 3080 (2001).
16. A. Leonard, Phys. Fluids. **6**, 765 (1994).
17. G. S. Winckelmans and A. Leonard, J. Comput. Phys. **109**, 247 (1993).
18. A. Leonard, Annu. Rev. Fluid Mech. **17**, 523 (1985).
19. A. Leonard and K. Chua, Physica **D37**, 490 (1989).
20. D. Kivotides and A. Leonard, Europhys. Lett. **63**, 354 (2003).
21. D. R. Poole, H. Scoffield, C. F. Barenghi, and D. C. Samuels, J. Low Temp. Phys. **132**, 97 (2003).
22. C. F. Barenghi, R. L. Ricca, and D. C. Samuels, Physica **D157**, 197 (2001).